

Tuning Fermi liquids with polaritonic cavities

Riccardo Riolo,¹ Andrea Tomadin,¹ Giacomo Mazza,¹ Reza Asgari,^{2,3} Allan H. MacDonald,⁴ and Marco Polini^{1,5}

¹*Dipartimento di Fisica dell'Università di Pisa, Largo Bruno Pontecorvo 3, I-56127 Pisa, Italy*

²*Department of Physics, Zhejiang Normal University, Jinhua, Zhejiang 321004, China*

³*School of Quantum Physics and Matter, Institute for Research in Fundamental Sciences (IPM), Tehran 19395-5531, Iran*

⁴*Department of Physics, The University of Texas at Austin, Austin, TX 78712, USA*

⁵*ICFO-Institut de Ciències Fotòniques, The Barcelona Institute of Science and Technology, Av. Carl Friedrich Gauss 3, 08860 Castelldefels (Barcelona), Spain*

The question of whether or not passive sub-wavelength cavities can alter the properties of quantum materials is currently attracting a great deal of attention. In this Article we show that the Fermi liquid parameters of a two-dimensional metal are modified by cavity polariton modes, and that these changes can be monitored by measuring a paradigmatic magneto-transport phenomenon, Shubnikov–de Haas oscillations in a weak perpendicular magnetic field. This effect is intrinsic, and totally unrelated to disorder. As an illustrative example, we carry out explicit calculations of the quasiparticle velocity of graphene in a planar van der Waals cavity formed by natural hyperbolic crystals and metal gates. The largest effects of the cavity occur when the phonon polariton modes of the former match energetically the graphene plasmon. For typical graphene carrier densities this occurs in the Terahertz spectral range.

Introduction. Magnetic oscillation phenomena [1, 2] like the de Haas–van Alphen effect, oscillations of the magnetization of a metal, are a powerful probe of the physics of itinerant electron systems. The frequencies of de Haas–van Alphen oscillations, for example, are an historically important probe of the Fermi surfaces of metals [1]. In metallic two-dimensional electron systems (2DESs) strong magnetic oscillations appear in the longitudinal resistivity ρ_{xx} [3] (Shubnikov–de Haas (SdH) oscillations) at magnetic fields weaker than those at which the quantum Hall effect occurs. Importantly, these can be used to access the Landau Fermi liquid parameters [4–7] of 2DESs such as the quasiparticle effective mass m^* (or, equivalently, quasiparticle velocity v_F^*) and the interaction enhanced g -factor g^* . Measurements in ultra-clean systems, including 2DESs confined to silicon inversion layers [8–10], AlAs/AlGaAs quantum wells [11–14], GaAs/AlGaAs quantum wells [15–17], LaAlO₃/SrTiO₃ interfaces [18, 19], SiGe/Si/SiGe quantum wells [20], and atomically-thin materials [21–25], report large deviations of m^* and g^* from the non-interacting values m_e and g .

The aim of this Article is to investigate whether SdH oscillations are affected by the fluctuations of an electromagnetic field confined to a small volume of space by a sub-wavelength [26–28] optical cavity. The possibility of tailoring the ground state and transport properties of an electron system solely by altering the fluctuations of a *passive* cavity (i.e. a cavity in the absence of optical pumping) is clearly potentially exciting and has recently captured a great deal of attention [29–33].

In 2DESs, transport is a particularly convenient probe to monitor passive cavity tuning of many-electron properties. The pioneering theoretical work on cavity-induced modifications of magneto-transport has been performed by Ciuti and co-workers [34–36] and Rubio and co-workers [44]. Recent experiments [37–43] have shown that the magneto-transport properties of a 2DES in a GaAs/AlGaAs quantum well can be modified by coupling

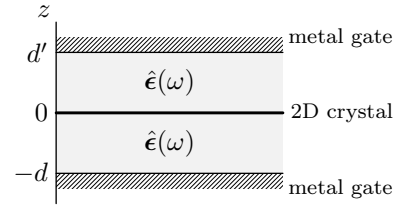


FIG. 1. A side view of the planar polaritonic cavity analyzed in this work. A 2D crystal which hosts a Fermi liquid (thick line) of areal density n_0 located at $z = 0$ is encapsulated between two hyperbolic dielectrics (light grey) described by frequency-dependent uniaxial permittivity tensors $\hat{\epsilon}(\omega) = \text{diag}(\epsilon_x(\omega), \epsilon_x(\omega), \epsilon_z(\omega))$. The bottom (top) slab has thickness d (d'). Metal gates (hatched grey) fill the two half-spaces $z > d'$ and $z < -d$. We assume that the dielectrics are identical.

the electronic degrees of freedom to sub-wavelength cavities in the Terahertz (THz) spectral range. In the case of split-ring THz resonators, for example, Ref. [42] reports a suppression of the amplitude of SdH traces, but no changes in the frequency B_F , in the passive regime.¹

Here we focus on the temperature (T) dependence of the SdH oscillations. According to the Lifshitz–Kosevich (LK) formula [45–49], the oscillatory component of the

¹ The experimental findings of Ref. [42] have been interpreted by using the theory of Ref. [34]. The latter deals with the static magneto-resistivity tensor of a 2DES coupled to a single cavity mode. In this theory, the authors take into account [34] the coupling between the cyclotron resonance of the 2DES and the cavity mode but neglect the temperature dependence of the amplitude of the SdH oscillations. We believe that any comparison between theory and experiment should take into account finite temperature effects, which strongly modify the amplitude of the SdH oscillations.

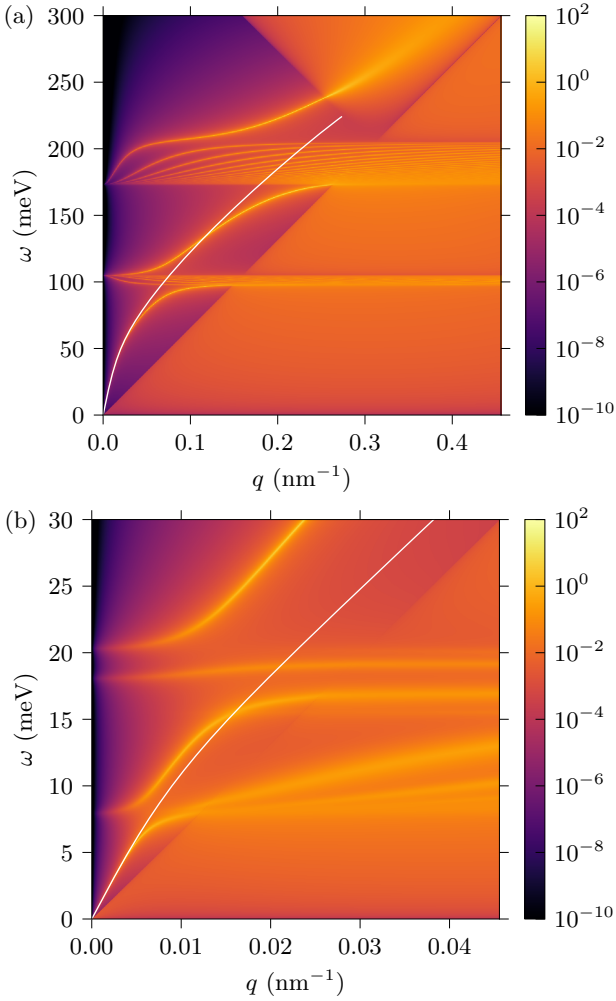


FIG. 2. Dynamical structure factor $S(q, \omega)$ (in units of k_F/v_F) as a function of the wave vector q and frequency ω . Results for graphene encapsulated by hBN—Panel (a)—and Bi_2Se_3 —Panel (b). In both panels, $n_0 = 3 \times 10^{12} \text{ cm}^{-2}$, and $d = d' = 50 \text{ nm}$ (parameters described in Fig. 1). The white solid line is the 2DES plasmon frequency calculated by artificially substituting $F(q, 0)$ for $F(q, \omega)$ in Eq. 4, thereby neglecting cavity dynamics. Notice that the plasmon dispersion is linear at small q because of the presence of metal gates (see Fig. 1).

magneto-resistance is given by²

$$\frac{\delta\rho_{xx}(B)}{\rho_0} = R(B, T) \cos\left(2\pi\left(\frac{B_F}{B} + \frac{1}{2} + \gamma\right)\right), \quad (1)$$

where ρ_0 is the resistance at $B = 0$, $B_F = \phi_0 n_0 / N_f$ is the frequency of the oscillations in $1/B$, $\phi_0 = hc/e$ is the magnetic flux quantum (c is the speed of light in vacuum and e the elementary charge), n_0 is the carrier density, N_f is a degeneracy factor, and $\gamma \in [0, 1)$ is a

² In writing Eq. (1), we have limited ourselves to the lowest harmonic.

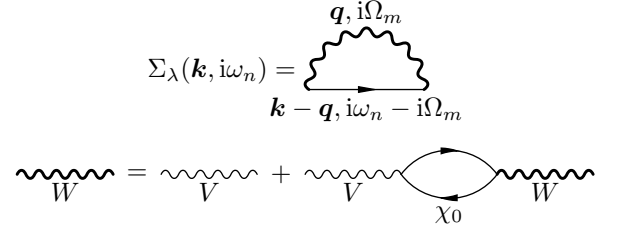


FIG. 3. Feynman diagrams considered in this work. Top: the irreducible self-energy $\Sigma_\lambda(\mathbf{k}, i\omega_n)$ in the G_0W approximation, Eq. (7). Bottom: the dynamically screened potential W in the random-phase approximation, as in Eq. (8). Here, V represents the Coulomb interaction *dressed by the cavity environment*, and χ_0 the polarization function of the 2DES.

Berry phase [50]. The amplitude $R(B, T)$ of the SdH oscillations is proportional to (and fully controlled by) the dimensionless quantity

$$A(B, T) = \frac{2\pi^2 k_B T / \hbar \omega_c}{\sinh(2\pi^2 k_B T / \hbar \omega_c)} e^{-\pi / \omega_c \tau}. \quad (2)$$

Here, τ is the momentum relaxation time, m_c the cyclotron mass, and $\omega_c \equiv eB/m_c c$ is the cyclotron frequency. The LK formula is derived under the assumptions of weak fields, i.e. $\hbar \omega_c \ll \mu$, where μ is the chemical potential. The τ -dependent Dingle factor [1] captures the reduction of the amplitude of the SdH oscillations due to electron-impurity scattering. Note that inelastic processes (such as electron-electron collisions) affect only $R(B, T)$ and not the SdH oscillation frequency B_F [1]. Eq. (2) is routinely used to fit the measured T -dependence of the amplitude of the SdH oscillations at a fixed value of B to extract an experimental value of m_c .

We now explain why and how SdH oscillations are modified by a sub-wavelength cavity. According to the LK formula (1), a passive cavity can act via both extrinsic and intrinsic microscopic mechanisms. The *extrinsic* mechanism is active if the cavity environment alters the momentum relaxation time τ with respect to the case where no cavity is present, and is clearly irrelevant in clean 2DES (i.e. for $\omega_c \tau \gg 1$). The intrinsic mechanism, which is the focus of this Article, is a cavity-induced change in the interaction-induced modification of the cyclotron mass m_c , which we evaluate as $m_c = \hbar k_F / v_F^*$, where k_F is the Fermi wave number and v_F^* is the quasiparticle velocity [7]. We show by explicit calculation that a sub-wavelength polaritonic cavity—such as the van der Waals cavity in Fig. 1—changes the quasiparticle weight factor Z and the renormalized Fermi velocity v_F^* of the normal Fermi liquid, relative to their values in vacuum. The reason is as follows: in the absence of the cavity, the spectrum or dynamical structure factor $S(q, \omega)$ of a clean 2DES displays a sharp plasmon mode, which carries a large fraction of the total f-sum rule spectral weight [5–7], and a continuum of particle-hole excitations. When coupling between the 2DES and the cavity is allowed, spectral weight flows from the electronic degrees of free-

dom to the polariton modes of the cavity, Fig. 2. This leads ultimately to changes in the Landau parameters of the 2DES.

Below, we first introduce a general theoretical framework, summarized in Fig. 3, that captures this physics and then present detailed calculations for the case of graphene embedded in the van der Waals cavity sketched in Fig. 1 containing metal gates and natural hyperbolic crystals [51–54], such as hexagonal Boron Nitride (hBN) [55–58] and Bi_2Se_3 [59].³ A specific illustration of the above mentioned spectral weight transfer is illustrated in Fig. 2, where we plot $S(q, \omega)$ [5–7] for graphene in the cavity shown in Fig. 1.

Polariton-mediated effective electron-electron interactions. We consider an interacting many-electron system embedded in a passive cavity, containing (hyperbolic) dielectric media and metal gates. Because condensed matter is only weakly relativistic, the coupling between matter and electromagnetic degrees of freedom can be separated [60] into non-radiative and radiative contributions. Non-radiative photons mediate density-density electron-electron interactions, while radiative ones mediate current-current interactions [61] that are weaker by $(v_F/c)^2$, where v_F is the bare Fermi velocity. For DC transport properties, the effects of photon-mediated density-density interactions is dominant with respect to the one of current-current interactions. (Current-current interactions can yield large modifications of response functions at *finite* frequency [62, 63], but have negligible effects on static properties. In the static limit, current-current interactions reduce to classical magneto-statics [64–67].)

After integrating out cavity degrees of freedom, the effective density-density interaction between electrons in a sub-wavelength cavity is given by $V(\mathbf{r}, \mathbf{r}', \omega) = e^2 g^{(s)}(\mathbf{r}, \mathbf{r}', \omega)$, where $g^{(s)}(\mathbf{r}, \mathbf{r}', \omega)$ [61, 68]⁴ is the scalar Green’s function for the frequency-dependent Poisson equation [2]:

$$-\partial_\alpha [\epsilon_{\alpha\beta}(\mathbf{r}, \omega) \partial_\beta \phi(\mathbf{r}, \omega)] = 4\pi \rho^{\text{ext}}(\mathbf{r}, \omega). \quad (3)$$

Here, $\phi(\mathbf{r}, \omega)$ is the electrical potential, $\rho^{\text{ext}}(\mathbf{r}, \omega)$ is the external charge density, and $\epsilon_{\alpha\beta}(\mathbf{r}, \omega)$ is the frequency-dependent complex permittivity tensor of the dielectric environment, which is assumed to be local in space.⁵

³ In this work we neglect the role of the surface states of the topological insulator slabs above and below graphene. Our interest in Bi_2Se_3 here is solely linked to its THz optical properties.

⁴ Green’s functions are routinely used [2] to quantify the role of vacuum fluctuations as long as one is interested in electromagnetic fields that vary slowly on the atomic scale. The most famous example [2] is probably the Lifshitz theory of the Casimir-Polder forces.

⁵ Spatial non-locality is important to describe chiral cavities [69] and will not be taken into account in this work. Here, indeed, we neglect the effect of spatial dispersion since we are interested in the phonon polariton modes of natural hyperbolic materials, which are very well described by our local approximation.

Losses enter the problem via the imaginary part of the permittivity tensor. Metal gates can be included by imposing [70] that, at metal-dielectric interfaces, the tangential component of the electric field vanishes and the normal component of the displacement field is $4\pi\sigma$, where σ is the surface charge density. Eq. (3) can be rigorously derived [61] in the generalized Coulomb gauge [71].

$V(\mathbf{r}, \mathbf{r}', \omega)$ describes the interaction between two charges at positions \mathbf{r} and \mathbf{r}' . In free space, it reduces to the ordinary, instantaneous Coulomb interaction [70], i.e. $v(|\mathbf{r} - \mathbf{r}'|) = e^2/|\mathbf{r} - \mathbf{r}'|$. In a sub-wavelength cavity, however, it can be vastly different from $v(|\mathbf{r} - \mathbf{r}'|)$. In particular, phonon polaritons in the metallo-dielectric cavity environment yield a retarded frequency-dependent interaction. In the $\omega = 0$ limit, $V(\mathbf{r}, \mathbf{r}', 0)$ physically describes static screening due to polarization charges in the metallo-dielectric environment. At finite ω , $V(\mathbf{r}, \mathbf{r}', \omega)$ encodes the polariton modes of the latter (including losses), which appear as poles of $V(\mathbf{r}, \mathbf{r}', z)$ viewed as a function of the complex frequency z .

Given $V(\mathbf{r}, \mathbf{r}', \omega)$, one can understand how the properties of the interacting many-electron system change due to the presence of the passive cavity by simply replacing the bare Coulomb interaction $v(|\mathbf{r} - \mathbf{r}'|)$ with the retarded interaction $V(\mathbf{r}, \mathbf{r}', \omega)$ in the framework of diagrammatic many-body perturbation theory [6, 7, 72]. This leads to generalized Hedin equations, from which one can calculate, for example, the one-body electron Green’s function $G(\mathbf{r}, \mathbf{r}', \omega)$, the irreducible self-energy [6, 7, 72] $\Sigma(\mathbf{r}, \mathbf{r}', \omega)$, and the density-density response function [6, 7] $\chi_{nn}(\mathbf{r}, \mathbf{r}', \omega)$. Poles in the latter quantity occur at the collective excitation energies of the 2DES/cavity hybrid system.

Illustrative example: a planar vdW polaritonic cavity. In order to illustrate the power of the approach we just described—while keeping the treatment of the cavity at a fully analytical level—we focus in what follows on a planar sub-wavelength cavity based on a vdW heterostructure [73], which is sketched in Fig. 1. The active material, where one measures magneto-transport, is a 2D crystalline material located at $z = 0$. This is encapsulated between two homogeneous and uniaxial dielectric slabs of different thicknesses, the slab on top (bottom) having thickness d' (d). The electrical permittivity tensor of these dielectrics is $\hat{\epsilon}(\omega) = \text{diag}(\epsilon_x(\omega), \epsilon_x(\omega), \epsilon_z(\omega))$. Note, finally, the presence of top and bottom metal gates. Without uniaxial dielectrics we would be dealing with an ordinary Fabry-Pérot cavity [61].

Setups like the one in Fig. 1 are routinely fabricated in laboratories throughout the world. The most studied case [73] is the one in which the 2D material is single-layer or Bernal-stacked bilayer graphene and the dielectric material is hBN [55–58]. Infinite possibilities are clearly possible: many other 2D conducting materials can be chosen (including twisted 2D materials) as well as low-loss dielectrics. For illustration purposes, below we will focus on single-layer graphene (SLG) encapsulated between two natural hyperbolic dielectrics [51–54].

In order to find $V(\mathbf{r}, \mathbf{r}', \omega)$ *analytically*, we follow an approach first proposed by Keldysh [74] and recently used in Ref. [75] in the context of vdW heterostructures. Since the setup in Fig. 1 is translationally invariant in the \hat{x} – \hat{y} plane, the scalar Green's function $g^{(s)}(z, z', |\mathbf{r}_\parallel - \mathbf{r}'_\parallel|, \omega)$ depends only on $|\mathbf{r}_\parallel - \mathbf{r}'_\parallel|$. Here, \mathbf{r}_\parallel and \mathbf{r}'_\parallel denote 2D positions in the \hat{x} – \hat{y} plane. The effective electron-electron interaction (EEEI) that is relevant for the many-body physics of the 2DES located at $z = 0$ is $V(0, 0, |\mathbf{r}_\parallel - \mathbf{r}'_\parallel|, \omega) = e^2 g^{(s)}(0, 0, |\mathbf{r}_\parallel - \mathbf{r}'_\parallel|, \omega)$. We are therefore naturally led to introduce its 2D Fourier transform⁶ $V(q, \omega)$ with respect to $r \equiv |\mathbf{r}_\parallel - \mathbf{r}'_\parallel|$. Once again, the frequency dependence of $V(q, \omega)$ encodes all the information about polaritons while its $\omega \rightarrow 0$ limit [61] encodes the physics of static screening due to the presence of metal gates and polarization charges.

We find that the polariton-mediated propagator of the planar vdW cavity sketched in Fig. 1 is given by $V(q, \omega) \equiv v_q F(q, \omega)$, where $v_q \equiv 2\pi e^2/q$ is the non-retarded 2D Coulomb propagator [7] and

$$F(q, \omega) \equiv \frac{2 \sinh \left[q \sqrt{\frac{\epsilon_x(\omega)}{\epsilon_z(\omega)}} d \right] \sinh \left[q \sqrt{\frac{\epsilon_x(\omega)}{\epsilon_z(\omega)}} d' \right]}{\epsilon_z(\omega) \sqrt{\frac{\epsilon_x(\omega)}{\epsilon_z(\omega)}} \sinh \left[q \sqrt{\frac{\epsilon_x(\omega)}{\epsilon_z(\omega)}} (d + d') \right]} \quad (4)$$

is a form factor [75–78]⁷ due to the presence of the dielectrics and metal gates. Optical phonons in the dielectrics are responsible for the frequency dependence of $F(q, \omega)$. The components of the uniaxial dielectric tensor are usually parametrized via a Lorentz oscillator model. In the case of a single mode, one has

$$\epsilon_\ell(\omega) = \epsilon_\ell(\infty) + \frac{\epsilon_\ell(0) - \epsilon_\ell(\infty)}{1 - (\omega/\omega_\ell^T)^2 - i\gamma_\ell\omega/(\omega_\ell^T)^2}, \quad (5)$$

with $\ell = x$ or z . Here, $\epsilon_\ell(0)$ and $\epsilon_\ell(\infty)$ are the static and high-frequency dielectric constants, respectively, while ω_ℓ^T is the transverse optical phonon frequency in the direction ℓ . The longitudinal optical phonon frequency ω_ℓ^L satisfies the Lyddane–Sachs–Teller relation $\omega_\ell^L = \omega_\ell^T \sqrt{\epsilon_\ell(0)/\epsilon_\ell(\infty)}$. The quantity γ_ℓ physically describes losses in the dielectric. Eq. (5) describes hBN accurately and realistic values of the parameters can be found e.g. in Ref. [76]. Multi-mode parametrizations of $\epsilon_\ell(\omega)$ for Bi₂Se₃ can be found in Ref. [59].

An inspection of Eq. (5) in the limit $\gamma_\ell \rightarrow 0$ shows that a dielectric described by this frequency-dependent

permittivity tensor is hyperbolic: in the lower (upper) reststrahlen band, which is defined by the inequality $\omega_z^T < \omega < \omega_z^L$ ($\omega_x^T < \omega < \omega_x^L$), the quantity $\epsilon_x(\omega)/\epsilon_z(\omega)$ takes negative values. Inside the reststrahlen bands, the dressed propagator $V(q, \omega)$ therefore displays poles, which physically correspond to standing hyperbolic phonon polaritons (SHPPs). In the case of negligible losses (i.e. for $\gamma_\ell = 0$), they can be found by looking at the zeroes of the denominator in Eq. (4):

$$q_n(\omega) = n \frac{\pi}{(d + d') \sqrt{|\epsilon_x(\omega)/\epsilon_z(\omega)|}}, \quad (6)$$

with $n = 1, 2, \dots$ ⁸. Note that the polariton wavelength $\lambda_p \equiv 2\pi/q_n(\omega) \ll \lambda_0$, where $\lambda_0 = 2\pi(c/\omega)$ is the free-space wavelength. The fact that $\lambda_p/\lambda_0 \ll 1$ is a distinctive feature of sub-wavelength polaritonic cavities. We now proceed to quantify how the Landau parameters of single-layer graphene (SLG) are modified by these modes.

Fermi liquid theory in a graphene cQED setup. The Landau parameters of a normal Fermi liquid are controlled by the one-body electron Green's function [6, 7, 72]. In a (massless Dirac fermion) continuum-model of SLG [80], the physical (i.e. retarded) electron Green's function $G_\lambda^{\text{ret}}(\mathbf{k}, \omega)$ is a function of a conserved wave vector \mathbf{k} and depends on a band index $\lambda = \pm$. It satisfies the Dyson equation (setting $\hbar = 1$), $G_\lambda^{\text{ret}}(\mathbf{k}, \omega) = [\omega - \xi_{\mathbf{k}, \lambda} - \Sigma_\lambda^{\text{ret}}(\mathbf{k}, \omega)]^{-1}$, where $\xi_{\mathbf{k}, \lambda} = \lambda v_F \mathbf{k} - \mu$ are single-particle band energies measured from the chemical potential μ and $\Sigma_\lambda^{\text{ret}}(\mathbf{k}, \omega)$ is the retarded self-energy [6, 7]. The latter quantity needs to be approximated. In a normal Fermi liquid, a good approximation is the so-called *G0W* approximation [6, 7, 72, 81–83]⁹ in which the electron self-energy is expanded to *first* order in the dynamically screened Coulomb interaction $W(q, i\Omega)$. The latter is approximated at the level of the random phase approximation (RPA) [6, 7]. The corresponding Feynman diagrams are displayed in Fig. 3. (The same approximation can be used when translational invariance is not at play [72] and G , Σ , and W depend on \mathbf{r} , \mathbf{r}' , and ω .)

In the case of SLG, the continuum-model *G0W* self-

⁶ The 2D Fourier transform is $V(q, \omega) \equiv \int d^2\mathbf{r} e^{-i\mathbf{q} \cdot \mathbf{r}} V(0, 0, r, \omega)$.

⁷ Eq. (4) has been derived by treating the top and bottom metal gates as perfect conductors. The authors of Ref. [79] transcended the perfect conductor approximation. This is relevant in the case of graphite gates or, more in general, when $q_{\text{TF}}d$ and $q_{\text{TF}}d'$ are small parameters. Here, q_{TF} is the Thomas-Fermi screening wave number [7] of the metal gate, which is proportional to the metal's density of states. The perfect conductor approximation is asymptotically exact in the limit $q_{\text{TF}}d, q_{\text{TF}}d' \rightarrow \infty$.

⁸ The poles of $V(q, \omega)$ are described by Eq. (6) if and only if d and d' are incommensurate. On the contrary, if $d/d' = m/m'$, the numerator has zeros when n is an integer multiple of $(m + m')$ and $V(q, \omega)$ has no poles for such values of n .

⁹ In the history of the theory of weakly-correlated electron liquids (such as 3D and 2D parabolic-bands electron gases and graphene), a plethora of authors has brought up the issue of whether or not one should calculate the Green's function self-consistently. An account of these interesting discussions can be found in Chapter 8 of Ref. [7]. The summary of these investigations is that, when vertex corrections are neglected as in the *G0W* approximation, it is much better to *avoid* self-consistency. For a 3D electron gas see, for example Ref. [84]. Self-consistent calculations, indeed, tend to yield an increase in the quasiparticle weight Z and broad (rather than sharp) plasmon satellites, in contradiction with experimental data.

energy [85, 86]

$$\Sigma_\lambda(\mathbf{k}, i\omega_n) = -k_B T \sum_{\lambda'} \int \frac{d^2 \mathbf{q}}{(2\pi)^2} \sum_{m=-\infty}^{+\infty} W(\mathbf{q}, i\Omega_m) \times F_{\lambda\lambda'}(\theta_{\mathbf{k}, \mathbf{k}-\mathbf{q}}) G_{\lambda'}^{(0)}(\mathbf{k} - \mathbf{q}, i\omega_n - i\Omega_m), \quad (7)$$

where $\omega_n = (2n + 1)\pi k_B T$ is a fermionic Matsubara frequency, the sum runs over all the bosonic Matsubara frequencies $\Omega_m = 2m\pi k_B T$, $F_{\lambda\lambda'}(\theta_{\mathbf{k}, \mathbf{k}-\mathbf{q}}) = [1 + \lambda\lambda' \cos(\theta_{\mathbf{k}, \mathbf{k}-\mathbf{q}})]/2$ is the SLG chirality factor, $\theta_{\mathbf{k}, \mathbf{k}-\mathbf{q}}$ is the angle between \mathbf{k} and $\mathbf{k} - \mathbf{q}$, $G_\lambda^{(0)}(\mathbf{k}, i\omega_n) = 1/(i\omega_n - \xi_{\mathbf{k}, \lambda})$ is the non-interacting temperature Green's function, and

$$W(\mathbf{q}, i\Omega) = \frac{V(\mathbf{q}, i\Omega)}{1 - V(\mathbf{q}, i\Omega)\chi_0(\mathbf{q}, i\Omega)} \quad (8)$$

is the dynamically screened interaction on the imaginary frequency axis. Here, $\chi_0(\mathbf{q}, i\Omega)$ is the SLG non-interacting density-density response function, evaluated on the imaginary-frequency axis [87]. The validity of this non-self-consistent G_0W approximation for graphene has been accurately checked against ARPES experimental data, see e.g. Refs. [88, 89].

We emphasize that the G_0W theoretical framework presented in Eqs. (7, 8) is valid also in the presence of losses in the cavity. In this case, however, care needs to be exercised in defining the quantities that enter Eq. (8). Indeed, any thermal Green's function $O(i\Omega)$ satisfies [2]

$$O(i\Omega) = \begin{cases} O^{\text{ret}}(i\Omega), & \text{for } \Omega > 0, \\ O^{\text{adv}}(i\Omega), & \text{for } \Omega < 0, \end{cases} \quad (9)$$

where $O^{\text{ret}}(\omega)$ and $O^{\text{adv}}(\omega)$ are the corresponding retarded and advanced Green's functions, respectively. Note that, $O^{\text{adv}}(z) = [O^{\text{ret}}(z^*)]^*$.

We also introduce the retarded density-density response function in the RPA approximation

$$\chi_{nn}(q, \omega) = \frac{\chi_0(q, \omega)}{1 - V(q, \omega)\chi_0(q, \omega)}, \quad (10)$$

where $\chi_0(q, \omega)$ is the non-interacting (retarded) polarization function on the real-frequency axis [90–92] and the polariton-mediated EEEI $V(q, \omega)$ has been introduced above. The dynamical structure factor $S(q, \omega)$ plotted in Fig. 2 is related to $\chi_{nn}(q, \omega)$ by the fluctuation-dissipation theorem [5–7], i.e. $S(q, \omega) = -(\hbar/\pi)\Theta(\omega)\text{Im}\chi_{nn}(q, \omega)$, where $\Theta(\omega)$ is the Heaviside step function.

Note that we can express $W(q, i\Omega)$ in Eq. (8) as:

$$W(q, i\Omega) = V(q, i\Omega) + V^2(q, i\Omega)\chi_{nn}(q, i\Omega). \quad (11)$$

The first term in the previous equation is responsible for the exchange interaction between a quasiparticle at the Fermi energy and the occupied Fermi sea. The second

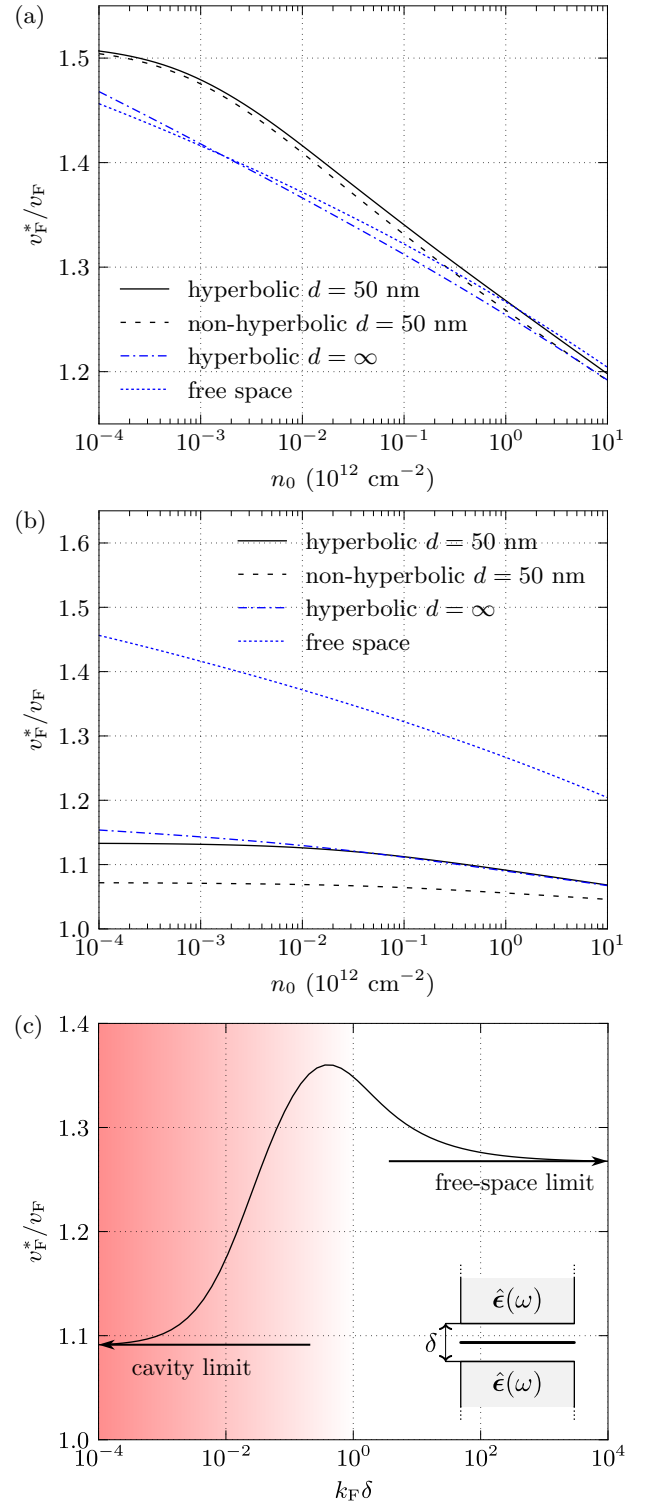


FIG. 4. Plot of the quasiparticle Fermi velocity v_F^*/v_F defined in Eqs. (13, 16a, 16b, 16c) as a function of the electron density n_0 for (a) hBN and (b) Bi₂Se₃. In both cases, $d' = d$ and the values of d have been indicated in the legend. Panel (c) shows v_F^*/v_F as a function of the dimensionless parameter $k_F \delta$ where δ is the distance between two semi-infinite ($d = d' \rightarrow \infty$) Bi₂Se₃ slabs. The inset shows the device configuration. As in Fig. 1, the thick black line represents graphene. No metal gates are present in this device. For $k_F \delta \gg 1$, we recover the results labelled by “free space” in panel (b). For $k_F \delta \lesssim 1$ the bulk polariton modes in Bi₂Se₃ couple strongly to the graphene plasmon and this is therefore the polaritonic “cavity QED” regime studied in this work. For $k_F \delta \rightarrow 0$, we recover the results labelled by “hyperbolic $d = \infty$ ” in panel (b).

term, instead, represents the interaction with particle-hole and *collective* virtual fluctuations. Both terms are dressed by SHPPs.

Landau Fermi liquid parameters are controlled by the physical (i.e. retarded) self-energy $\Sigma_+^{\text{ret}}(\mathbf{k}, \omega)$, which can be obtained from the analytical continuation $i\omega_n \rightarrow \omega + i0^+$ from imaginary to real frequencies. For definiteness, we consider the case of electron-doped SLG with positive chemical potential μ (results for $\mu < 0$ are identical because of particle-hole symmetry). The quasiparticle weight factor Z and the renormalized Fermi velocity v_F^* (in units of the bare value v_F) can be expressed in terms of the wave-vector and frequency derivatives of the retarded self-energy $\Sigma_+^{\text{ret}}(\mathbf{k}, \omega)$ evaluated at the Fermi surface ($k = k_F$) and at the quasiparticle pole $\omega = \xi_+(\mathbf{k})$ [6, 7]:

$$Z = \frac{1}{1 - \partial_\omega \text{Re} \Sigma_+^{\text{ret}}(\mathbf{k}, \omega)|_{k=k_F, \omega=0}}, \quad (12)$$

$$\frac{v_F^*}{v_F} = \frac{1 + (v_F)^{-1} \partial_k \text{Re} \Sigma_+^{\text{ret}}(\mathbf{k}, \omega)|_{k=k_F, \omega=0}}{1 - \partial_\omega \text{Re} \Sigma_+^{\text{ret}}(\mathbf{k}, \omega)|_{k=k_F, \omega=0}}. \quad (13)$$

Following some standard manipulations [7, 81], the retarded self-energy can be expressed in a form convenient for numerical evaluation, as the sum $\Sigma_\lambda^{\text{ret}}(\mathbf{k}, \omega) = \Sigma_\lambda^{\text{res}}(\mathbf{k}, \omega) + \Sigma_\lambda^{\text{line}}(\mathbf{k}, \omega)$ of a contribution from the interaction of quasiparticles at the Fermi energy, the *residue* contribution $\Sigma_\lambda^{\text{res}}(\mathbf{k}, \omega)$, and a contribution from interactions with quasiparticles far from the Fermi energy and via both exchange and virtual fluctuations, the *line* contribution $\Sigma_\lambda^{\text{line}}(\mathbf{k}, \omega)$. In the zero-temperature limit

$$\begin{aligned} \Sigma_\lambda^{\text{res}}(\mathbf{k}, \omega) &= \sum_{\lambda'=\pm} \int \frac{d^2\mathbf{q}}{(2\pi)^2} W(q, \omega - \xi_{\lambda'}(\mathbf{k} - \mathbf{q})) \\ &\times F_{\lambda\lambda'}(\theta_{\mathbf{k}, \mathbf{k}-\mathbf{q}}) [\Theta(\xi_{\lambda'}(\mathbf{k} - \mathbf{q})) - \Theta(\xi_{\lambda'}(\mathbf{k} - \mathbf{q}) - \omega)] \end{aligned} \quad (14)$$

and

$$\begin{aligned} \Sigma_\lambda^{\text{line}}(\mathbf{k}, \omega) &= - \sum_{\lambda'=\pm} \int \frac{d^2\mathbf{q}}{(2\pi)^2} F_{\lambda\lambda'}(\theta_{\mathbf{k}, \mathbf{k}-\mathbf{q}}) \\ &\times \int_{-\infty}^{+\infty} \frac{d\Omega}{2\pi} \frac{W(\mathbf{q}, i\Omega)}{\omega - i\Omega - \xi_{\lambda'}(\mathbf{k} - \mathbf{q})}. \end{aligned} \quad (15)$$

In what follows we will calculate the following three quantities:

$$\left. \frac{v_F^*}{v_F} \right|_{\text{free space}} \equiv \left. \frac{v_F^*}{v_F} \right|_{F(q, \omega) \rightarrow 1}, \quad (16a)$$

$$\left. \frac{v_F^*}{v_F} \right|_{\text{non-hyperbolic}} \equiv \left. \frac{v_F^*}{v_F} \right|_{F(q, \omega) \rightarrow F(q, 0)}, \quad (16b)$$

$$\left. \frac{v_F^*}{v_F} \right|_{\text{hyperbolic}} \equiv \left. \frac{v_F^*}{v_F} \right|_{F(q, \omega)}. \quad (16c)$$

The quantity in Eq. (16a) physically represents the quasiparticle Fermi velocity (measured in units of the

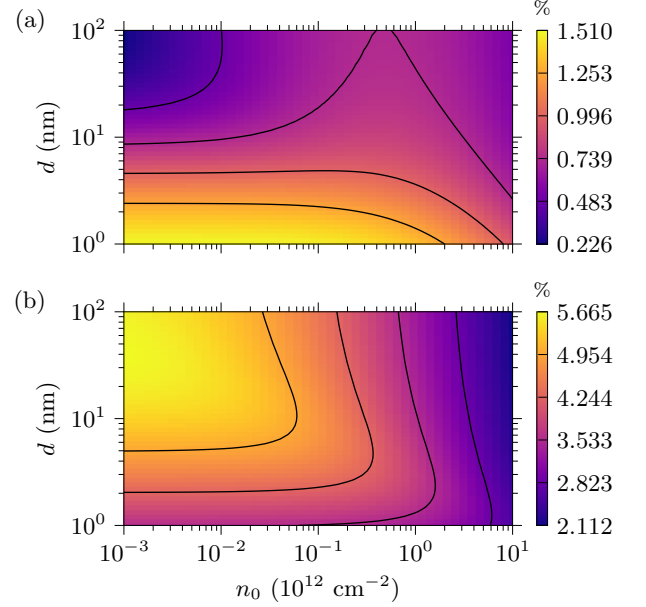


FIG. 5. Cavity QED effect on the quasiparticle Fermi velocity v_F^* . Color plots of Δ_{QED} —as defined in Eq. (17)—as a function of the electron density n_0 and dielectric thickness $d = d'$. Panel (a): the case of hBN. Panel (b): the case of Bi_2Se_3 .

bare Fermi velocity v_F) in graphene, in the total absence of screening stemming from nearby dielectrics and metal gates. It is mathematically calculated by forcing the full dynamical propagator $V(q, \omega)$ to coincide with the instantaneous Coulomb free-space propagator, i.e. $V(q, \omega) \rightarrow v_q$. The quantity $v_F^*|_{\text{free space}}$ is clearly measurable [23].

The quantity in Eq. (16b) physically represents the quasiparticle Fermi velocity (in units of v_F) in a graphene sheet embedded in the cavity sketched in Fig. 1. However, it is calculated by forcing $V(q, \omega)$ to attain its static value, i.e. $V(q, \omega) \rightarrow V(q, 0) = v_q F(q, 0)$. The quantity in Eq. (16b) therefore includes static screening from the dielectrics and top/bottom metal gates. Notice that: i) in the $V(q, \omega) \rightarrow V(q, 0)$ limit, top and bottom dielectrics are *not* hyperbolic and ii) $v_F^*|_{\text{non-hyperbolic}}$ is not measurable but it is an important theoretical construct, as emphasized below.

Finally, the quantity in Eq. (16c) is the quasiparticle Fermi velocity (in units of v_F) in a graphene sheet embedded in the cavity sketched in Fig. 1 and calculated with the full retarded propagator $V(q, \omega)$. This last quantity includes the role of SHPPs.

Numerical results and discussion. We now present our main numerical results. In Fig. 4 we show the dependence of the quasiparticle Fermi velocity v_F^* (in units of $v_F = 10^6$ m/s) on carrier density n_0 , for $d = d' = 50$ nm. Panel (a) in this figure refers to SLG encapsulated in hBN. In this case and at high electron densities, the value of v_F^* calculated with the retarded EEEI $V(q, \omega)$ differs little from the result $v_F^*|_{\text{free space}}$ obtained

with the instantaneous Coulomb interaction v_q . In the intermediate-to-low density regime (i.e. for $10^8 \text{ cm}^{-2} < n_0 < 10^{11} \text{ cm}^{-2}$), however, the density dependence of $v_{\text{F}}^*|_{\text{hyperbolic}}$ is different from that of $v_{\text{F}}^*|_{\text{free space}}$. While the latter displays the González-Guinea-Vozmediano logarithmic growth [23, 80], the former saturates to a constant value. This is a qualitative effect, which may be verified experimentally, stemming from the different dependence of $V(q, \omega)$ on q with respect to the bare 2D Coulomb interaction v_q . While v_q behaves as $1/q$ at any length scale, $V(q, \omega)$ is strongly screened by the metallic gates and saturates to constant value in the limit $dk_{\text{F}}, d'k_{\text{F}} \rightarrow 0$, i.e. $\lim_{dk_{\text{F}}, d'k_{\text{F}} \rightarrow 0} V(q, \omega) = 4\pi e^2 dd' / [\epsilon_z(\omega)(d + d')]$. Going to densities lower than 10^8 cm^{-2} (i.e. approaching the charge neutrality point $n_0 = 0$), the logarithmic growth of $v_{\text{F}}^*|_{\text{free space}}$ overwhelms the saturating behavior of $v_{\text{F}}^*|_{\text{hyperbolic}}$.

In Fig. 4 we also present results for the asymptotic regime $d = d' \rightarrow \infty$ (distance between the metal gates is sent to infinity). The fact that the effect of SHPPs persists also in this limit indicates that polariton-mediated cavity QED effects do not require the presence of metallic mirrors and is peculiar to the case of density-density interactions. In the case of current-current interactions mediated by radiative photons [93], fingerprints of SHPPs disappear in the limit $d = d' \rightarrow \infty$ (see Fig. 3 of Ref. [93]). Since the effect persists in the absence of metallic mirrors, the reader may wonder why we talk about “cavity” effects. The key point is that, in our setup, the dielectric slabs precisely act as cavity mirrors that modify the properties of the material placed in between them by shaping the electromagnetic vacuum in the vicinity of the material. To see this, we introduce a new length scale in the problem, i.e. the distance δ between the top and bottom dielectric slabs in the limit $d = d' \rightarrow \infty$, and place the graphene halfway between the dielectrics¹⁰—see the inset in Fig. 4(c). In the main body of Fig. 4(c) we show the “cavity” effect, i.e. the fact that we can tune the quasiparticle velocity v_{F}^* by tuning the distance δ between the two dielectric slabs. Indeed, for $\delta \rightarrow \infty$, the polariton modes do not couple to the graphene plasmon and one recovers the “free space” limit—see Eq. (16a). Viceversa, tuning δ towards the $k_{\text{F}}\delta \lesssim 1$ regime, boosts the strength of the plasmon-polariton coupling, yielding the strongest renormalization of the Fermi velocity.

An important figure of merit to quantify the role of virtual polaritonic excitations (i.e. the role of genuine QED effects) on the quasiparticle Fermi velocity is the

following:

$$\Delta_{\text{QED}} = \frac{v_{\text{F}}^*|_{\text{hyperbolic}} - v_{\text{F}}^*|_{\text{non-hyperbolic}}}{v_{\text{F}}^*|_{\text{non-hyperbolic}}}. \quad (17)$$

The larger Δ_{QED} the larger the role of virtual SHPPs. The smaller Δ_{QED} the larger is the (trivial) role of static screening from polarization charges in the dielectric and metal gates. In other words, large values of Δ_{QED} certify that changes in the quasiparticle Fermi velocity in a given cavity are not a trivial consequence of static screening. Of course, we have checked that, in the device configuration shown in the inset of Fig. 4(c), $\Delta_{\text{QED}} \rightarrow 0$ in the limit $k_{\text{F}}\delta \gg 1$.

The quantity Δ_{QED} is plotted in Fig. 5(a) for the case of SLG encapsulated in hBN. We clearly see that Δ_{QED} is small, on the order of 1.5% at best, and weakly dependent on n_0 and dielectric thickness d . We believe that the reason is that hBN reststrahlen bands occur at very high energies, the lower one starting at $\omega = \omega_z^{\text{T}} \simeq 97 \text{ meV}$. On the contrary, the SLG plasmon carries a large spectral weight (in fact, the total spectral weight) at small values of q and $\omega > v_{\text{F}}q$. This “mismatch” in the (q, ω) plane between the SLG plasmon and the hBN (lower) reststrahlen band suppresses spectral flow from the matter degrees of freedom to the phonon polariton ones.

To show that this is indeed the case, we have also calculated the quasiparticle Fermi velocity v_{F}^* for SLG encapsulated in Bi_2Se_3 . Results for this case are reported in Fig. 4(b). We immediately see that the cavity plays a much stronger role, both at the static and polaritonic levels. The fact that $v_{\text{F}}^*|_{\text{non-hyperbolic}}$ is much smaller than $v_{\text{F}}^*|_{\text{free space}}$ stems from the fact that Bi_2Se_3 has a much smaller band gap than hBN, and therefore much larger values of the static in-plane and out-of-plane permittivities. The fact that $v_{\text{F}}^*|_{\text{hyperbolic}}$ is larger than $v_{\text{F}}^*|_{\text{non-hyperbolic}}$ is due to the fact that Bi_2Se_3 has reststrahlen bands at much lower energies, the lower one occurring at energies on the order of 8 meV.¹¹ Fig. 5 shows the quantity Δ_{QED} as a function of system parameters.

¹⁰ In the case of the device geometry illustrated in Fig. 4(c), the electromagnetic form factor has the following expression:

$$F(q, \omega) = \frac{\epsilon_z(\omega) \sqrt{\frac{\epsilon_x(\omega)}{\epsilon_z(\omega)}} \cosh \left[q \sqrt{\frac{\epsilon_x(\omega)}{\epsilon_z(\omega)}} \frac{\delta}{2} \right] + \sinh \left[q \sqrt{\frac{\epsilon_x(\omega)}{\epsilon_z(\omega)}} \frac{\delta}{2} \right]}{\epsilon_z(\omega) \sqrt{\frac{\epsilon_x(\omega)}{\epsilon_z(\omega)}} \sinh \left[q \sqrt{\frac{\epsilon_x(\omega)}{\epsilon_z(\omega)}} \frac{\delta}{2} \right] + \cosh \left[q \sqrt{\frac{\epsilon_x(\omega)}{\epsilon_z(\omega)}} \frac{\delta}{2} \right]}.$$

¹¹ At these low energies, one may worry about thermal occupation of the phonon-polariton modes. Since 8 meV corresponds to a temperature on the order of 100 K, in order to measure the quasiparticle velocity v_{F}^* of graphene without worrying about these thermal effects, SdH oscillations need to be measured up to a maximum temperature $T_{\text{max}} \sim 100 \text{ K}$. In order to extract v_{F}^* from a fit of the T -dependence of the amplitude of the SdH oscillations, one also needs to make sure that in the $0 \text{ K} < T < 100 \text{ K}$ range, $A(B, T)$ changes appreciably. From Eq. (2), we see that $A(B, T)$ decreases by a factor of 10 when the argument of the hyperbolic sinus is $2\pi^2 k_{\text{B}} T / \hbar \omega_c \sim 5$. Thus, the highest T one should reach is estimated to be $T_{\text{theory}} \sim (5eBv_{\text{F}}) / (2\pi^{5/2} k_{\text{B}} c |n|^{1/2})$. In SI units, $T_{\text{theory}} \sim (\bar{B} |\bar{n}|^{-1/2}) 20 \text{ K}$, where \bar{B} is the applied magnetic field in Tesla and \bar{n} the carrier density in units of 10^{12} cm^{-2} . For typical densities and applied magnetic fields [21, 23], this theoretical estimate is also on the order of 100 K. We can therefore neglect thermal occupation of phonon-polariton modes in the case of Bi_2Se_3 .

Without fine tuning, the QED effect on the quasiparticle Fermi velocity is much larger in this cavity rather than in the case of hBN.

A systematic quest of hyperbolic dielectrics with reststrahlen bands at ultra-low energies in order to maximize Δ_{QED} is beyond the scope of the present Article. Nevertheless, our work shows that measurable QED effects emerge in DC magneto-transport in planar van der Waals cavities. We expect that these effects can be greatly enhanced in cavities where SHPPs and matter degrees of freedom are subject to lateral (and not only vertical) confinement, as in the case of Ref. [94]. Recently developed on-chip THz spectroscopy [95] may also be used to reveal strong coupling effects in van de Waals heterostructures. From a theoretical point of view, it will be very interesting to extend the theory presented in this work to (a) real and moiré crystals and (b) strongly correlated materials [96].

Data, Materials, and Software Availability. The data that support the findings of this article are openly avail-

able [97].

Acknowledgements. M. P. wishes to thank G. M. Andolina, M. Ceccanti, F. H. L. Koppens, and A. R. Hamilton for many useful discussions. R. R. and A. T. acknowledge the “National Centre for HPC, Big Data and Quantum Computing” under the National Recovery and Resilience Plan (NRRP), Mission 4 Component 2 Investment 1.4 CUP I53C22000690001 funded from the European Union – NextGenerationEU. G. M. was supported by the Rita-Levi Montalcini program of the MUR. A. H. M. was supported by a grant from the Keck foundation. M. P. was supported by the European Union’s Horizon 2020 research and innovation programme under the Marie Skłodowska-Curie grant agreement No. 873028 - Hydrotronics and by the MUR - Italian Minister of University and Research under the “Research projects of relevant national interest - PRIN 2020” - Project No. 2020JLZ52N, title “Light-matter interactions and the collective behavior of quantum 2D materials (q-LIMA)”.

-
- [1] D. Shoenberg, *Magnetic Oscillations in Metals* (Cambridge University Press, Cambridge, 1984).
 - [2] L. D. Landau and E. M. Lifshitz, *Course of Theoretical Physics: Statistical Physics, Part 2* (Pergamon, New York, 1980).
 - [3] T. Ando, A. B. Fowler, and F. Stern, Electronic properties of two-dimensional systems, *Rev. Mod. Phys.* **54**, 437 (1982).
 - [4] T. M. Rice, The effects of electron-electron interaction on the properties of metals, *Ann. Phys. (N.Y.)* **31**, 100 (1965).
 - [5] D. Pines and P. Nozières, *The Theory of Quantum Liquids* (W.A. Benjamin, Inc., New York, 1966).
 - [6] G. D. Mahan, *Many-Particle Physics, Third Edition* (Plenum Publishers, New York, 2000).
 - [7] G. F. Giuliani and G. Vignale, *Quantum Theory of the Electron Liquid* (Cambridge University Press, Cambridge, 2005).
 - [8] F. F. Fang and P. J. Stiles, Effects of a tilted magnetic field on a two-dimensional electron gas, *Phys. Rev.* **174**, 823 (1968).
 - [9] J. L. Smith and P. J. Stiles, Electron-electron interactions continuously variable in the range $2.1 > r_s > 0.9$, *Phys. Rev. Lett.* **29**, 102 (1972).
 - [10] V. M. Pudalov, M. E. Gershenson, H. Kojima, N. Butch, E. M. Dizhur, G. Brunthaler, A. Prinz, and G. Bauer, Low-density spin susceptibility and effective mass of mobile electrons in Si inversion layers, *Phys. Rev. Lett.* **88**, 196404 (2002).
 - [11] K. Vakili, Y. P. Shkolnikov, E. Tutuc, E. P. De Poortere, and M. Shayegan, Spin susceptibility of two-dimensional electrons in narrow AlAs quantum wells, *Phys. Rev. Lett.* **92**, 226401 (2004).
 - [12] M. Padmanabhan, T. Gokmen, N. C. Bishop, and M. Shayegan, Effective mass suppression in dilute, spin-polarized two-dimensional electron systems, *Phys. Rev. Lett.* **101**, 026402 (2008).
 - [13] T. Gokmen, M. Padmanabhan, and M. Shayegan, Dependence of effective mass on spin and valley degrees of freedom, *Phys. Rev. Lett.* **101**, 146405 (2008).
 - [14] T. Gokmen, M. Padmanabhan, K. Vakili, E. Tutuc, and M. Shayegan, Effective mass suppression upon complete spin-polarization in an isotropic two-dimensional electron system, *Phys. Rev. B* **79**, 195311 (2009).
 - [15] Y.-W. Tan, J. Zhu, H. L. Stormer, L. N. Pfeiffer, K. W. Baldwin, and K. W. West, Measurements of the density-dependent many-body electron mass in two dimensional GaAs/AlGaAs heterostructures, *Phys. Rev. Lett.* **94**, 016405 (2005).
 - [16] Y.-W. Tan, J. Zhu, H. L. Stormer, L. N. Pfeiffer, K. W. Baldwin, and K. W. West, Spin susceptibility and effective mass of a 2D electron system in GaAs heterostructures towards the weak interacting regime, *Physica E: Low Dimens. Syst. Nanostruct.* **34** 260 (2006).
 - [17] YenTing Chiu, M. Padmanabhan, T. Gokmen, J. Shabani, E. Tutuc, M. Shayegan, and R. Winkler, Effective mass and spin susceptibility of dilute two-dimensional holes in GaAs, *Phys. Rev. B* **84**, 155459 (2011).
 - [18] A. D. Caviglia, S. Gariglio, C. Cancellieri, B. Sacépé, A. Fête, N. Reyren, M. Gabay, A. F. Morpurgo, and J.-M. Triscone, Two-dimensional quantum oscillations of the conductance at LaAlO₃/SrTiO₃ interfaces, *Phys. Rev. Lett.* **105**, 236802 (2010).
 - [19] M. Ben Shalom, A. Ron, A. Palevski, and Y. Dagan, Shubnikov-de Haas oscillations in LaAlO₃/SrTiO₃ interface, *Phys. Rev. Lett.* **105**, 206401 (2010).
 - [20] M. Yu. Melnikov, A. A. Shakirov, A. A. Shashkin, S. H. Huang, C. W. Liu, and S. V. Kravchenko, Spin independence of the strongly enhanced effective mass in ultra-clean SiGe/Si/SiGe two-dimensional electron system, *Sci. Rep.* **13**, 17364 (2023).
 - [21] K. S. Novoselov, A. K. Geim, S. V. Morozov, D. Jiang, M. I. Katsnelson, I. V. Grigorieva, S. V. Dubonos, and A. A. Firsov, Two-dimensional gas of massless Dirac fermions in graphene, *Nature* **438**, 197 (2005).

- [22] Y. Zhang, Y.-W. Tan, H. L. Stormer, and P. Kim, Experimental observation of the quantum Hall effect and Berry's phase in graphene, *Nature* **438**, 201 (2005).
- [23] D. C. Elias, R. V. Gorbachev, A. S. Mayorov, S. V. Morozov, A. A. Zhukov, P. Blake, L. A. Ponomarenko, I. V. Grigorieva, K. S. Novoselov, F. Guinea, and A. K. Geim, Dirac cones reshaped by interaction effects in suspended graphene, *Nat. Phys.* **7**, 701 (2011).
- [24] K. Zou, X. Hong, and J. Zhu, Effective mass of electrons and holes in bilayer graphene: Electron-hole asymmetry and electron-electron interaction, *Phys. Rev. B* **84**, 085408 (2011).
- [25] B. Fallahazad, H. C. P. Movva, K. Kim, S. Larentis, T. Taniguchi, K. Watanabe, S. K. Banerjee, and E. Tutuc, Shubnikov-de Haas oscillations of high-mobility holes in monolayer and bilayer WSe₂: Landau level degeneracy, effective mass, and negative compressibility, *Phys. Rev. Lett.* **116**, 086601 (2016).
- [26] L. Novotny and B. Hecht, *Principles of Nano-Optics, Second Edition* (Cambridge University Press, Cambridge, 2012).
- [27] D. N. Basov, A. Asenjo-Garcia, P. J. Schuck, X. Zhu, and A. Rubio, Polariton panorama, *Nanophoton.* **10**, 549 (2021).
- [28] A. Reserbat-Plantey, I. Epstein, I. Torre, A. T. Costa, P. A. D. Gonçalves, N. A. Mortensen, M. Polini, J. C. W. Song, N. M. R. Peres, and F. H. L. Koppens, Quantum nanophotonics in two-dimensional materials, *ACS Photon.* **8**, 85 (2021).
- [29] J. Bloch, A. Cavalleri, V. Galitski, M. Hafezi, and A. Rubio, Strongly correlated electron-photon systems, *Nature* **606**, 41 (2022).
- [30] F. Schlawin, D. M. Kennes, and M. A. Sentef, Cavity quantum materials, *Appl. Phys. Rev.* **9**, 011312 (2022).
- [31] F. J. Garcia-Vidal, C. Ciuti, and T. W. Ebbesen, Manipulating matter by strong coupling to vacuum fields, *Science* **373**, 6551 (2021).
- [32] C. Genet, J. Faist, and T. Ebbesen, Inducing new material properties with hybrid light-matter states, *Phys. Today* **74**, 42 (2021).
- [33] H. Hübener, U. De Giovannini, C. Schäfer, J. Andberger, M. Ruggenthaler, J. Faist, and A. Rubio, Engineering quantum materials with chiral optical cavities, *Nat. Mater.* **20**, 438 (2021).
- [34] N. Bartolo and C. Ciuti, Vacuum-dressed cavity magnetotransport of a two-dimensional electron gas, *Phys. Rev. B* **98**, 205301 (2018).
- [35] C. Ciuti, Cavity-mediated electron hopping in disordered quantum Hall systems, *Phys. Rev. B* **104**, 155307 (2021).
- [36] G. Arwas and C. Ciuti, Quantum electron transport controlled by cavity vacuum fields, *Phys. Rev. B* **107**, 045425 (2023).
- [37] G. Scalari, C. Maissen, D. Turcinková, D. Hagenmüller, S. De Liberato, C. Ciuti, C. Reichl, D. Schuh, W. Wegscheider, M. Beck, and J. Faist, Ultrastrong coupling of the cyclotron transition of a 2D electron gas to a THz metamaterial, *Science* **335**, 1323 (2012).
- [38] V. M. Muravev, P. A. Gusikhin, I. V. Andreev, and I. V. Kukushkin, Ultrastrong coupling of high-frequency two-dimensional cyclotron plasma mode with a cavity photon, *Phys. Rev. B* **87**, 045307 (2013).
- [39] C. Maissen, G. Scalari, F. Valmorra, M. Beck, J. Faist, S. Cibella, R. Leoni, C. Reichl, C. Charpentier, and W. Wegscheider, Ultrastrong coupling in the near field of complementary split-ring resonators, *Phys. Rev. B* **90**, 205309 (2014).
- [40] S. Smolka, W. Wuester, F. Haupt, S. Faelt, W. Wegscheider, and A. Imamoglu, Cavity quantum electrodynamics with many-body states of a two-dimensional electron gas, *Science* **346**, 332 (2014).
- [41] J. Keller, G. Scalari, S. Cibella, C. Maissen, F. Appugliese, E. Giovine, R. Leoni, M. Beck, and J. Faist, Few-electron ultrastrong light-matter coupling at 300 GHz with nanogap hybrid LC microcavities, *Nano Lett.* **17**, 7410 (2017).
- [42] G. L. Paravicini-Bagliani, F. Appugliese, E. Richter, F. Valmorra, J. Keller, M. Beck, N. Bartolo, C. Rössler, T. Ihn, K. Ensslin, C. Ciuti, G. Scalari, and J. Faist, Magneto-transport controlled by Landau polariton states, *Nat. Phys.* **15**, 186 (2019).
- [43] F. Appugliese, J. Enkner, G. L. Paravicini-Bagliani, M. Beck, C. Reichl, W. Wegscheider, G. Scalari, C. Ciuti, and J. Faist, Breakdown of topological protection by cavity vacuum fields in the integer quantum Hall effect, *Science* **375**, 6584 (2022).
- [44] V. Rokaj, J. Wang, J. Sous, M. Penz, M. Ruggenthaler, and A. Rubio, Weakened Topological Protection of the Quantum Hall Effect in a Cavity, *Phys. Rev. Lett.* **131**, 196602 (2023).
- [45] I. M. Lifshitz and A. M. Kosevich, Theory of Magnetic Susceptibility in Metals at Low Temperatures, *Zh. Eksp. Teor. Fiz.* **29**, 730 (1955) [*Sov. Phys. JETP* **2**, 636 (1956)].
- [46] A. Isihara and L. Smrčka, Density and magnetic field dependences of the conductivity of two-dimensional electron systems, *J. Phys. C* **19**, 6777 (1986).
- [47] S. G. Sharapov, V. P. Gusynin, and H. Beck, Magnetic oscillations in planar systems with the Dirac-like spectrum of quasiparticle excitations, *Phys. Rev. B* **69**, 075104 (2004).
- [48] I. A. Luk'yanchuk and Y. Kopelevich, Phase analysis of quantum oscillations in graphite, *Phys. Rev. Lett.* **93**, 166402 (2004).
- [49] C. Küppersbusch and L. Fritz, Modifications of the Lifshitz-Kosevich formula in two-dimensional Dirac systems, *Phys. Rev. B* **96**, 205410 (2017).
- [50] G. P. Mikitik and Yu. V. Sharlai, Manifestation of Berry's phase in metal physics, *Phys. Rev. Lett.* **82**, 2147 (1999).
- [51] J. Sun, N. M. Litchinitser, and J. Zhou, Indefinite by nature: From ultraviolet to terahertz, *ACS Photon.* **1**, 293 (2014).
- [52] D. N. Basov, M. M. Fogler, and F. J. G. de Abajo, Polaritons in van der Waals materials, *Science* **354**, aag1992 (2016).
- [53] T. Low, A. Chaves, J. D. Caldwell, A. Kumar, N. X. Fang, P. Avouris, T. F. Heinz, F. Guinea, L. Martin-Moreno, and F. Koppens, Polaritons in layered two-dimensional materials, *Nat. Mater.* **16**, 182 (2017).
- [54] Q. Zhang, G. Hu, W. Ma, P. Li, A. Krasnok, R. Hiltenbrand, A. Alù, and C.-W. Qiu, Interface nano-optics with van der Waals polaritons, *Nature* **597**, 187 (2021).
- [55] S. Dai, Z. Fei, Q. Ma, A. S. Rodin, M. Wagner, A. S. McLeod, M. K. Liu, W. Gannett, W. Regan, K. Watanabe, T. Taniguchi, M. Thiemens, G. Dominguez, A. H. Castro Neto, A. Zettl, F. Keilmann, P. Jarillo-Herrero, M.M. Fogler, and D. N. Basov, Tunable phonon polaritons in atomically thin van der Waals crystals of boron nitride, *Science* **343**, 1125 (2014).

- [56] J. D. Caldwell, A. Kretinin, Y. Chen, V. Giannini, M. M. Fogler, Y. Francescato, C. T. Ellis, J. G. Tischler, C. R. Woods, A. J. Giles, M. Hong, K. Watanabe, T. Taniguchi, S. A. Maier, and K. S. Novoselov, Sub-diffractive volume-confined polaritons in the natural hyperbolic material hexagonal boron nitride, *Nat. Commun.* **5**, 5221 (2014).
- [57] P. Li, M. Lewin, A. V. Kretinin, J. D. Caldwell, K. S. Novoselov, T. Taniguchi, K. Watanabe, F. Gaussmann, and T. Taubner, Hyperbolic phonon-polaritons in boron nitride for near-field optical imaging and focusing, *Nat. Commun.* **6**, 7507 (2015).
- [58] S. Dai, Q. Ma, T. Andersen, A. S. McLeod, Z. Fei, M. K. Liu, M. Wagner, K. Watanabe, T. Taniguchi, M. Thiemens, F. Keilmann, P. Jarillo-Herrero, M. M. Fogler, and D. N. Basov, Subdiffractive focusing and guiding of polaritonic rays in a natural hyperbolic material, *Nat. Commun.* **6**, 6963 (2015).
- [59] E. A. A. Pogna, L. Viti, A. Politano, M. Brambilla, G. Scamarcio, and M. S. Vitiello, Mapping propagation of collective modes in Bi_2Se_3 and $\text{Bi}_2\text{Te}_{2.2}\text{Se}_{0.8}$ topological insulators by near-field terahertz nanoscopy, *Nat. Commun.* **12**, 6672 (2021).
- [60] C. Cohen-Tannoudji, J. Dupont-Roc, and G. Grynberg, *Photons and Atoms: Introduction to Quantum Electrodynamics* (Wiley-VCH, Berlin, 1997).
- [61] G. M. Andolina, A. De Pasquale, F. M. D. Pellegrino, I. Torre, F. H. L. Koppens, and M. Polini, Amperean superconductivity cannot be induced by deep subwavelength cavities in a two-dimensional material, *Phys. Rev. B* **109**, 104513 (2024).
- [62] J. Flick, D. M. Welakuh, M. Ruggenthaler, H. Appel, and A. Rubio, Light-matter response in nonrelativistic quantum electrodynamics, *ACS Photon.* **6**, 2757 (2019).
- [63] I. Amelio, L. Korosec, I. Carusotto, and G. Mazza, Optical dressing of the electronic response of two-dimensional semiconductors in quantum and classical descriptions of cavity electrodynamics, *Phys. Rev. B* **104**, 235120 (2021).
- [64] P. Nataf, T. Champel, G. Blatter, and D. M. Basko, Rashba cavity QED: A route towards the superradiant quantum phase transition, *Phys. Rev. Lett.* **123**, 207402 (2019).
- [65] G. M. Andolina, F. M. D. Pellegrino, V. Giovannetti, A. H. MacDonald, and M. Polini, Theory of photon condensation in a spatially varying electromagnetic field, *Phys. Rev. B* **102**, 125137 (2020).
- [66] D. Guerici, P. Simon, and C. Mora, Superradiant phase transition in electronic systems and emergent topological phases, *Phys. Rev. Lett.* **125**, 257604 (2020).
- [67] G. Mazza and M. Polini, Hidden excitonic quantum states with broken time-reversal symmetry, *Phys. Rev. B* **108**, L241107 (2023).
- [68] A. Asenjo-Garcia, J. D. Hood, D. E. Chang, and H. J. Kimble, Atom-light interactions in quasi-one-dimensional nanostructures: A Green's-function perspective, *Phys. Rev. A* **95**, 033818 (2017).
- [69] L. D. Landau and E. M. Lifshitz, *Course of Theoretical Physics: Electrodynamics of Continuous Media* (Pergamon, New York, 1984).
- [70] J. D. Jackson, *Classical Electrodynamics, Third Edition* (Wiley, New York, 1999).
- [71] R. J. Glauber and M. Lewenstein, Quantum optics of dielectric media, *Phys. Rev. A* **43**, 467 (1991).
- [72] L. Hedin and S. Lundqvist, Effects of electron-electron and electron-phonon interactions on the one-electron states of solids, *Solid State Phys.* **23**, 1 (1969).
- [73] A. Geim and I. Grigorieva, Van der Waals heterostructures, *Nature* **499**, 419 (2013).
- [74] L. V. Keldysh, Coulomb interaction in thin semiconductor and semimetal films, *Pis'ma Zh. Eksp. Teor. Fiz.* **29**, 716 (1979).
- [75] A. Tomadin, A. Principi, J. C. W. Song, L. S. Levitov, and M. Polini, Accessing phonon polaritons in hyperbolic crystals by angle-resolved photoemission spectroscopy, *Phys. Rev. Lett.* **115**, 087401 (2015).
- [76] A. Woessner, M. B. Lundeberg, Y. Gao, A. Principi, P. Alonso-González, M. Carrega, K. Watanabe, T. Taniguchi, G. Vignale, M. Polini, J. Hone, R. Hillenbrand, and F. H. L. Koppens, Highly confined low-loss plasmons in graphene-boron nitride heterostructures, *Nat. Mater.* **14**, 421 (2015).
- [77] M. B. Lundeberg, Y. Gao, R. Asgari, C. Tan, B. Van Duppen, M. Autore, P. Alonso-González, A. Woessner, K. Watanabe, T. Taniguchi, R. Hillenbrand, J. Hone, M. Polini, and F. H. L. Koppens, Tuning quantum nonlocal effects in graphene plasmonics, *Science* **357**, 187 (2017).
- [78] P. Alonso-González, A. Y. Nikitin, Y. Gao, A. Woessner, M. B. Lundeberg, A. Principi, N. Forcellini, W. Yan, S. Vélez, A. J. Huber, K. Watanabe, T. Taniguchi, F. Casanova, L. E. Hueso, M. Polini, J. Hone, F. H. L. Koppens, and R. Hillenbrand, Ultra-confined acoustic THz graphene plasmons revealed by photocurrent nanoscopy, *Nat. Nanotech.* **12**, 31 (2017).
- [79] M. Kim, S. G. Xu, A. I. Berdyugin, A. Principi, S. Slizovskiy, N. Xin, P. Kumaravadevel, W. Kuang, M. Hamer, R. Krishna Kumar, R. V. Gorbachev, K. Watanabe, T. Taniguchi, I. V. Grigorieva, V. I. Fal'ko, M. Polini, and A. K. Geim, Control of electron-electron interaction in graphene by proximity screening, *Nat. Commun.* **11**, 2339 (2020).
- [80] V. N. Kotov, B. Uchoa, V. M. Pereira, F. Guinea, and A. H. Castro Neto, Electron-electron interactions in graphene: current status and perspectives, *Rev. Mod. Phys.* **84**, 1067 (2012).
- [81] J. J. Quinn and R. A. Ferrell, Electron self-energy approach to correlation in a degenerate electron gas, *Phys. Rev.* **112**, 812 (1958).
- [82] L. Hedin, New method for calculating the one-particle Green's function with application to the electron-gas problem, *Phys. Rev.* **139**, A796 (1965).
- [83] M. S. Hybertsen and S. G. Louie, Electron correlation in semiconductors and insulators: Band gaps and quasiparticle energies, *Phys. Rev. B* **34**, 5390 (1986).
- [84] B. Holm and U. von Barth, Fully self-consistent GW self-energy of the electron gas, *Phys. Rev. B* **57**, 2108 (1998).
- [85] M. Polini, R. Asgari, Y. Barlas, T. Pereg-Barnea, and A. H. MacDonald, Graphene: a pseudo-chiral Fermi liquid, *Solid State Commun.* **143**, 58 (2007).
- [86] M. Polini, R. Asgari, G. Borghi, Y. Barlas, T. Pereg-Barnea, and A. H. MacDonald, Plasmons and the spectral function of graphene, *Phys. Rev. B* **77**, 081411(R) (2008).
- [87] Y. Barlas, T. Pereg-Barnea, M. Polini, R. Asgari, and A. H. MacDonald, Chirality and correlations in graphene, *Phys. Rev. Lett.* **98**, 236601 (2007).
- [88] A. Bostwick, F. Speck, T. Seyller, K. Horn, M. Polini, R. Asgari, A. H. MacDonald, and E. Rotenberg, Ob-

- servation of Plasmarons in Quasi-Freestanding Doped Graphene, *Science* **328**, 999 (2010).
- [89] A. L. Walter, A. Bostwick, K. Jeon, F. Speck, M. Ostler, T. Seyller, L. Moreschini, Y. J. Chang, M. Polini, R. Asgari, A. H. MacDonald, K. Horn, and E. Rotenberg, Effective screening and the plasmaron bands in graphene, *Phys. Rev. B* **84**, 085410 (2011).
- [90] K. W.-K. Shung, Dielectric function and plasmon structure of stage-1 intercalated graphite, *Phys. Rev. B* **34**, 979 (1986).
- [91] B. Wunsch, T. Stauber, F. Sols, and F. Guinea, Dynamical polarization of graphene at finite doping, *New J. Phys.* **8**, 318 (2006).
- [92] E. H. Hwang and S. Das Sarma, Dielectric function, screening, and plasmons in two-dimensional graphene, *Phys. Rev. B* **75**, 205418 (2007).
- [93] Y. Ashida, A. İmamoğlu, and E. Demler, Cavity quantum electrodynamics with hyperbolic van der Waals materials, *Phys. Rev. Lett.* **130**, 216901 (2023).
- [94] H. H. Sheinfux, L. Orsini, M. Jung, I. Torre, M. Ceccanti, S. Marconi, R. Maniyara, D. Barcons Ruiz, A. Hötger, R. Bertini, S. Castilla, N. C. H. Hesp, E. Janzen, A. Holleitner, V. Pruneri, J. H. Edgar, G. Shvets, and F. H. L. Koppens, High quality nanocavities through multimodal confinement of hyperbolic polaritons in hexagonal boron nitride, *Nat. Mater.* **23**, 499 (2024).
- [95] G. Kipp, H. M. Bretscher, B. Schulte, D. Herrmann, K. Kussyak, M. W. Day, S. Kesavan, T. Matsuyama, X. Li, S. M. Langner, J. Hagelstein, F. Sturm, A. M. Potts, C. J. Eckhardt, Y. Huang, K. Watanabe, T. Taniguchi, A. Rubio, D. M. Kennes, M. A. Sentef, E. Baudin, G. Meier, M. H. Michael, and J. W. McIver, Cavity electrodynamics of van der Waals heterostructures, [arXiv:2403.19745](https://arxiv.org/abs/2403.19745).
- [96] E. G. C. P. van Loon, M. Schüler, D. Springer, G. Sangiovanni, J. M. Tomczak, and T. O. Wehling, Coulomb engineering of two-dimensional Mott materials, *npj 2D Mater. Appl.* **7**, 47 (2023) and references therein.
- [97] Software used to produce the plots in this article is available at Zenodo <https://zenodo.org/records/15874135>.